Lithuanian Journal of Physics
Vol. **63**, No. 4, pp. 241–250 (2023)
ISSN 1648-8504 eISSN 2424-3647
DOI: https://doi.org/10.3952/physics.2023.63.4.6

# SUPERSTRATE-LENS INTEGRATION USING PARAFFIN WAX ON TOP OF SEMICONDUCTOR-BASED THz DETECTOR CHIPS

**H. Yuan, Q. ul-Islam, and H.G. Roskos**

*Physikalisches Institut, Goethe-Universität Frankfurt am Main, 60438 Frankfurt am Main, Germany*
Email: yuan@physik.uni-frankfurt.de; roskos@physik.uni-frankfurt.de

Received 14 November 2023; accepted 15 November 2023

A detector of electromagnetic radiation may benefit – if its sensor area is small – from the application of a substrate lens, which focusses the radiation onto the active sensing area of the device and thus enhances its responsivity. The use of such a lens, attached directly onto the detector backside in order to avoid reflection losses, requires that the detector substrate and backside be transparent to the radiation. However, if this is not the case, one may like to place instead a superstrate lens onto the front side of the detector. It may even be of interest to use both a substrate and a superstrate lens if the detector needs to be illuminated with two beams, e.g. for heterodyne detection, where one beam provides the local-oscillator signal. The use of a superstrate lens is, however, often hindered or impeded by an uneven surface topography or by the presence of bonding wires on the front side of the detector. Here, we address this issue and explore the use of paraffin wax to form or attach superstrate lenses. In the first case, which is the main topic of this contribution, we exploit the surface tension of liquid paraffin, brought onto the detector, to sculpt the wax itself into a lens. In the second case, only addressed conceptually here, we use paraffin to form a thin intermediate layer which also acts as an adhesive for the attachment of a plastic or silicon lens. In both cases, the application of liquid paraffin allows one to fill out an uneven detector surface and to embed wires without breaking them. We investigate the use of wax for the case of CMOS TeraFETs – detectors of terahertz radiation based on field-effect transistors – embedded into antenna structures. We describe the processing steps and analyze the performance of a TeraFET equipped with such a wax superstrate lens for front-side beam coupling.

**Keywords:** THz detection, THz coupling, heterodyne detection

## 1. Introduction

Terahertz (THz) technology holds promise for numerous industrial applications in areas such as security monitoring [1], medicine [2], aerospace [3], communications [4] and automotive sensing [5]. In comparison to more mature microwave and optical technologies, the early challenges in the development of THz technology revolved around the achievement of an effective emission and detection of THz radiation. In recent years, thanks to dedicated efforts by researchers and the continuously improved use of micro-manufacturing processes, relatively compact THz sources [6] and sensitive detection [7] methods have emerged, at least for such an application where only a single detector is required. However, for certain applications such as THz imaging, a higher radiation power, respectively, detector sensitivity remains to be desirable, if not necessary, depending on the specifics of the imaging task [8, 9]. A part of the challenge for THz imaging is relatively long wavelengths in the THz frequency range as compared with those in the optical range. Detector devices operating in the THz frequency band tend to be relatively large, making integration into arrays challenging. Even when using power-combining techniques with distributed sources as described in the literature [6], it remains challenging to achieve an imaging performance equivalent to that of the optical wavelength range. There is intensive research ongoing to develop imaging modalities which are well-adapted to the unique conditions of the THz spectral regime [8, 9]. Two approaches are to employ the spatial-spectral imaging techniques in the focal plane (the plane with the highest intensity) of the imaging system such as Fourier imaging [10, 11] and the compressed sensing-based single-pixel

techniques [12]. The better the sensitivity of detection with these techniques, the better the imaging dynamic range and resolution. Coherent detection [13] (which also makes the phase of the radiation available for image processing) is a powerful technology to achieve a high image quality, and an effective coupling of the radiation to the detector is being crucial for the successful implementation of coherent imaging.

The research presented here focusses on practical ways of improving the front-end coupling efficiency of THz semiconductor detectors based on Schottky diodes, field-effect transistors or related ones, which come integrated with metallic antennae. In the case of ground-plane-free antennae such as bowtie antennae or log-spiral antennae, radiation is typically coupled in through the substrate onto the detector backside (which clearly necessitates a good transparency of the substrate at the wavelength of radiation). In order to achieve a good efficiency, one applies a hemispherical or hyper-hemispherical lens to the substrate. The lens is usually made from high-resistivity Si. It has a dielectric constant at THz frequencies well matched to that of all semiconductor materials used for the implementation of THz detectors, which eliminates or at least minimizes reflection losses at the lens–substrate interface. However, for detectors integrated with an antenna requiring an embedded ground-plane such as patch antennae, this approach no longer works. Only front-side coupling is possible in this case (if one wants to avoid more complex side-coupling schemes, e.g. with waveguides). The attachment of a lens to the front side may be hindered by a possible surface topography of the detector, which may not allow one to bring the detector in a direct contact with the active region of the detector, but even more so by the presence of bonding wires used to connect the chip to the readout circuitry. With the application of the lens, one risks to break and disrupt the bonding wires. One is then often left with the option to couple the radiation in through air, which may result in a low coupling efficiency. But even when a ground-plane-free detector is employed, one may wish front-side coupling. This can, for example, be the case if the detector is used as a receiver for homodyne or heterodyne coherent detection [13–15], provided the local-oscillator (LO) wave reaches the detector in the form of free-space radiation. In this case, injecting the signal wave and the LO wave from opposite sides into the detector avoids losses at a beam combiner used to overlap the two beams if one couples both in from the same side.

To address this issue, a method is presented here that involves the integration of soft paraffin wax on the front-side of the semiconductor. With the paraffin, one can address three purposes: (i) to smoothen the front-side facet of the chip, (ii) to provide a base and attachment layer with a relatively high dielectric constant (2.3, for the measurements see below) for superstrate lens integration (which includes making a lens from the wax itself, see below), and (iii) to embed and thus protect the bonding wires of the detector in the wax.[1] Figure 1(a) depicts two schematic views of a detector equipped with a superstrate and a substrate lens. On the left side there is an exploded view, showcasing a paraffin wax layer serving both as the bonding-wire protection layer and as the 'glue' for the attachment of a superstrate lens which can consist either of a hard solid material such as Si or sapphire, a solid plastic material such as PTFE, or a shapeable material such as paraffin wax itself. In the example of Fig. 1(a), a Si substrate lens is attached to the backside of a Si carrier wafer onto which a detector chip is mounted. We have recently used such an arrangement for subharmonic heterodyne detection, with backside-coupled signal radiation at 600 GHz and front-side-coupled LO radiation at 300 GHz [11, 16]. The right side of Fig. 1(a) schematically displays the assembled double-lens arrangement. In Fig. 1(b), we show two photographs of an actual implementation of the concept, with a paraffin wax lens sculptured into a quasi-spherical shape on the front-side of a detector chip and a Si substrate lens on the backside. The present paper primarily focusses on the fabrication and use of such hand-moulded paraffin wax lenses, an approach which stood at the beginning of our exploration of double-lens implementation on THz detectors and hence represents only the first-generation attempt to the task [17]. The investigation of wax-attached Si and PTFE lenses will be described in other publications.

Paraffin wax is a soft solid derived from petroleum, coal, or shale oil. It consists of a mixture of alkanes of different molecular weight. The molecular

[1] We note in passing that a paraffin wax layer with a quarter-wave thickness could also be used as an anti-reflection layer because the refractive index of the wax is intermediate between those of classical bulk semiconductors and air.

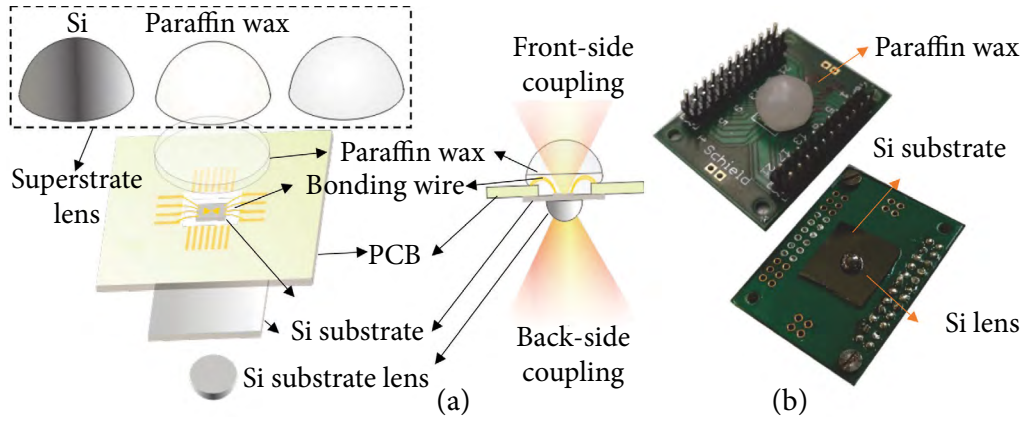


Fig. 1. (a) Schematic views of the disassembled and the fully integrated lens arrangement with paraffin wax material on a detector, and (b) photographs of the dual-lens-integrated detector with a paraffin-wax superstrate lens on the front-side and a Si substrate lens on the backside of the detector chip.

formula is $C_mH_{2m+2}$, where $m = 20 \sim 40$. It is solid at room temperature and melts above approximately 37°C (99°F) [18]. Common applications include lubrication, electrical insulation and the production of candles.

In the following, we first describe measurements of the dielectric properties of the paraffin wax material in the THz frequency band up to 2.5 THz. We then address the use of paraffin wax, starting from the dropcasting of molten paraffin wax onto the front-side of the detector for the embedding of bonding wires, followed by the preparation of the lens shape by employing, first, the surface tension of liquid wax and melt-sculpturing under the microscope afterwards. While this lens-crafting approach is rudimentary and certainly does not represent a process with the guaranteed reproducibility wanted for mature technology, it is still versatile and fairly quick to implement, and has the advantage that it leads to the lens arrangement consisting of a single material which eliminates concerns about reflection losses at the interface between different materials.

## 2. Dielectric properties of paraffin wax at THz frequencies

We investigated the dielectric properties of paraffin wax in the THz frequency range using the THz time-domain spectroscopy (TDS) system with a frequency bandwidth of 2.5 THz [19]. To prepare a sample, paraffin wax was melted and cast into a disk shape using a metal ring frame, resulting in a wax layer with a thickness of 2.44 mm, as measured with calipers. Figure 2(a) shows the THz transients measured with and without a sample in

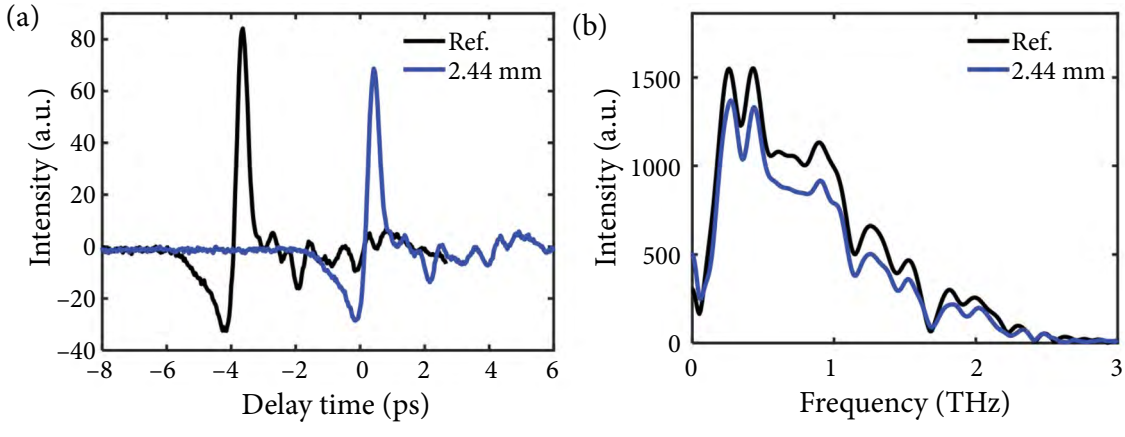


Fig. 2. (a) TDS THz transient after propagation through the wax disk (a blue curve), reference measurement (a black curve). (b) Frequency-domain intensity data.

the beam path (blue vs black curve), Fig. 2(b) presents the Fourier intensity spectra of TDS data.

The frequency-dependent real part $n(f)$ of the refractive index of the sample was determined by applying the formula [20]

$$n(f) = n_0 + \frac{c_0[\varphi_s(f) - \varphi_r(f)]}{2\pi fd}, \quad (1)$$

where $\varphi_s(f) - \varphi_r(f)$ is the frequency-dependent phase difference between the measurements with the sample and without one (the reference), $c_0$ is the speed of light, $d$ is the thickness of the sample, $n_0$ is the refractive index of air, and $f$ is the frequency. $\varphi_s(f) - \varphi_r(f)$ is obtained upon the Fourier transformation of time-domain data. The results are shown in Fig. 3.

The paraffin wax exhibits only a weak dispersion over the frequency range of 0.3 to 1.5 THz. The real part of the refractive index (the right vertical axis) shows a slight decrease with increasing frequency, starting at 1.52 at 300 GHz and decreasing to just above 1.5 at 1.5 THz. The average value is 1.515 across the range 0.3–1.5 THz.

The determination of the extinction coefficient $k(f)$ (the imaginary part of the refractive index), respectively, the absorption coefficient $\alpha(f) = 4\pi fk(f)/c_0$, generally requires reflection and transmission measurements. With TDS, transmission data are sufficient if time-delayed pulses arising from multiple reflections within the specimen can be separated clearly from the main transmitted pulse by time-windowing. For a weak absorption, one obtains [21]

$$\alpha(f) = -\frac{2}{d}\ln\left(\frac{(n(f)+n_0)^2}{4n(f)}\cdot t(f)\right). \quad (2)$$

Here, $t(f) = E_s(f)/E_r(f)$ is the transmission coefficient obtained from the Fourier transforms $E_s(f)$ and $E_r(f)$ of the transmitted electric fields with a sample and without one.

The absorption coefficient $\alpha(f)$ is plotted in Fig. 3 (the left vertical axis) over the frequency range 0.3–1.5 THz. The absorption at low frequency amounts to about 0.3–0.4 cm$^{-1}$. It gradually increases with rising frequency to 0.8 cm$^{-1}$. The absorption is hence reasonably low to allow the use of this wax material for the formation of superstrate lenses which have a thickness of significantly less than a centimetre. The modulations on the curve of the absorption coefficient in Fig. 3 arise from THz absorption by water vapour in the air (the THz beam path was unpurged) and (especially at the edges of the spectral range) from numerical artifacts of the Fourier analysis.

## 3. Estimation of the improvement of radiation coupling efficiency by superstrate lens

We now estimate the coupling efficiency of the incoming radiation to the detector without and with the superstrate lens. We assume that the lens is made entirely from paraffin wax. The overall coupling efficiency to the detector depends on the integral of field distribution on the effective area of the antenna and the matching efficiency of the antenna and the transistor. The latter is fixed for any specific chip design [22, 23]. We ignore the specifics

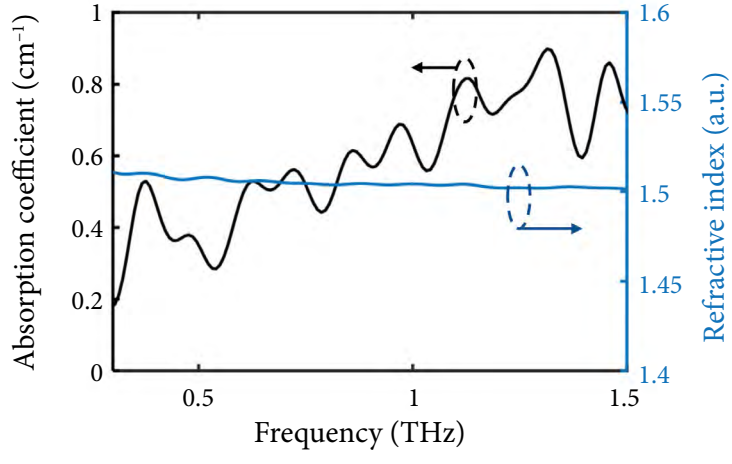


Fig. 3. Frequency dependence of the absorption coefficient and the refractive index of paraffin wax as determined by TDS.

of the external free-space optical system by assuming this beam-forming optics to be the same for beam coupling either through the air or the superstrate lens. The analysis therefore will only focus on the role of the effective detection area of the antenna vs the effective physical antenna size.

When the antenna of a detector is embedded at the interface of two half-infinite dielectric materials (which is conceptionally satisfied by the assumption of a detector embedded between a hemispherical paraffin-wax superstrate lens and a Si substrate lens), the ratio of the power received (respectively, radiated out) from either side can be roughly defined as $n_1^3/n_2^3$ ($n_1$ and $n_2$ being the refractive indices of dielectrics) [24]. The directivity for detection (emission) in the direction of the first dielectric is then found to be given by the expression $n_1^3/(n_2^3 + n_1^3) \cdot Dr$ ($Dr$ is the total antenna directivity). With the formula for the effective antenna area $Ar$ [25]

$$Ar = (Dr \cdot \lambda^2)/4\pi = (n_1 + n_2)\, A_{\text{antenna}}/2, \tag{3}$$

where $\lambda$ is the wavelength in vacuum and $A_{\text{antenna}}$ is the physical antenna area, the equivalent effective antenna area in the first dielectric is

$$A_1 = \frac{n_1^3 (n_2 + n_1)}{2(n_2^3 + n_1^3)} A_{\text{antenna}}. \tag{4}$$

If medium 1 is either air or paraffin wax, and medium 2 is silicon, then, in Eq. (4), $n_2$ should be substituted by $n_{\text{si}}$, and $n_1$ by $n_{\text{air}}$, respectively, $n_{\text{wax}}$ for the comparison of coupling either through the air or through the paraffin wax lens. Applying $n_{\text{Si}} \approx 3.45$ [26, 17], $n_{\text{air}} = 1$ and $n_{\text{wax}} = 1.52$ (see above), one finds that the effective antenna area, and with it the coupling efficiency of the radiation, is enhanced by a factor of 3.7 by the paraffin wax material. We do not address the influence of the shape of the lens on the coupling efficiency because of the imponderability of the manual lens-shape sculpturing described below.

In the case of heterodyne detection, the readout at the intermediate frequency (IF) is proportional to $[A_f A_{\text{LO}}^{*n}/(2^n n!)] \cos(2\pi \cdot \Delta f \cdot \text{t} + \Delta\varphi)$ [27] (where $A_f$ and $A_{\text{LO}}^{*n}$ represent the amplitudes of the signal and LO waves in the detector, * is the notation of conjugation, $n$ is the order of the subharmonic mixing, $\Delta f$ is the IF, and $\Delta\varphi$ denotes the phase difference between the signal and LO). The IF readout signal is heavily dependent on $A_{\text{LO}}^{*n}$. In our imaging work of [11, 16], we employed signal radiation at 600 GHz and LO radiation at 300 GHz for 2nd subharmonic heterodyne detection, hence $n = 2$. As a result, the improvement in sensitivity by the enhancement of the effective antenna area is squared in relation to the enhancement of the coupling efficiency of LO radiation.

## 4. Integration of a paraffin wax layer and lens formation on a broadband CMOS THz detector

We implemented a wax substrate lens on the frontside of a Si CMOS detector. The detector was an antenna-coupled field-effect transistor (TeraFET) [28] with a bow-tie antenna for broadband responsivity [29]. The detector was ready for use, mounted on a PCB board and wire-bonded to the bonding pads of the board (see Fig. 1(b)). The integration of the paraffin wax layer and the lens formation followed those steps: first, wax material is melted at a temperature of 120°C. At this temperature, the paraffin has a relatively low viscosity. When the molten wax is carefully dropped onto the frontside of the detector chip, it encloses the bonding wires, leaving no air bubbles. When the wires are embedded entirely, the temperature of the melt is reduced to 100°C. More wax is then dropped onto the assembly. As the cooler wax has a larger viscosity and a larger surface tension, it does not flow apart anymore, but forms a dome on the cooled wax under it. This dome is then sculpted into the desired lens shape centred exactly on the detector antenna. The lens centring (by reshaping) is performed under a microscope with a large working distance. When the wax is in its liquid state, it is transparent. To ensure an accurate alignment, the centre of the detector is aligned with the cross mark on the microscope, and the centre of the wax droplet is aligned with the mark. Achieving the proper shape of the lens requires practicing. For the measurements described below, the paraffin-wax lens has a bottom diameter of approximately 8 mm.

## 5. Application test with subharmonic heterodyne Fourier imaging at 600 GHz

The effect of the paraffin-wax superstrate lens on the THz detection efficiency was explored with the Fourier imaging system, where the dynamic range of detection plays a crucial role for the image

quality [16]. We show the imaging results for the object consisting of a two-dimensional planar metal grid with 2.5-mm-wide stripes and 5-mm-wide square openings (as shown in Fig. 4(a)). The metal grid was placed perpendicular to the collimated illumination beam. Figure 4(b) illustrates the principle of Fourier imaging in the transmission mode [8]. The continuous-wave THz beam, after having passed through the object, is focussed by a plastic lens. In the focal plane, the field pattern represents the spatial Fourier transform of the object multiplied with a phase factor which contains the information about the distance of the object from the principal plane of the lens. The amplitude and phase of the electric field in the focal plane is raster-scanned with a single-pixel detector operating in the subharmonic heterodyne mode. The image is then reconstructed numerically by applying an inverse Fourier transformation to the complex-valued spectrum and back-propagating the data to the original position of the object. A detailed description of the Fourier-imaging system and its operation can be found in Ref. [16].

Figure 5(a, b) displays the raw Fourier-plane spectra of the metal grid, recorded with and without a paraffin-wax superstrate lens for the LO radiation on the front-side of the detector, respectively. In both cases, the object-illuminating beam impinged onto the backside of the detector through the Si substrate lens. Figure 5(c) presents the reconstructed images based on the Fourier-plane spectrum of Fig. 5(a), while Fig. 5(d) depicts the corresponding reconstructions of the Fourier-plane spectrum shown in Fig. 5(b). In all figures, the left and right panels display the intensity and phase distributions, respectively. In the Fourier plane, the recorded data represent essentially (up to the additional propagation factor) the spatial spectrum, with each position in the Fourier plane corresponding to a $k$-vector (wave-vector). The farther away from the centre, the higher the absolute value of the $k$-vector. Higher $k$-vectors are important for a good spatial resolution in the reconstructed images. However, as the amplitudes of Fourier components typically decrease with rising the $k$-vector magnitude, the signal in the Fourier plane becomes weaker farther away from the centre.

From the Fourier-space spectra in Fig.5, it is evident that employing the paraffin-wax lens led to an improved data recording. With the substrate lens, the area with useful data (i.e. not noise-dominated data) is much larger in Fig. 5(a) than in Fig. 5(b), where only a small region around the centre is above the noise level. This, in turn, results in both an enhanced field-of-view (FOV) and a better spatial resolution in the reconstructed image (compare Fig. 5(c) with Fig. 5(d)). This improvement can be attributed to the successful collection of higher $k$-vector contributions enabled by a higher sensitivity of the THz detector equipped with the wax

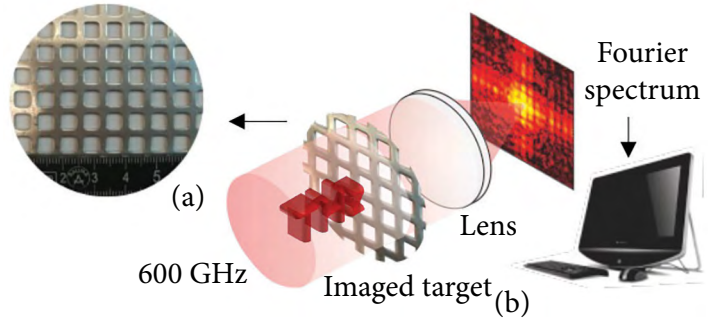


Fig. 4. Schematics of THz Fourier imaging. (a) Photograph of the metal grid used as a test object. (b) Simplified layout of the imaging system. The continuous-wave THz beam arrives from the left side (letters 'THz' in red), passes the object and the lens. The distribution of electric field in the focal plane (Fourier plane) of the lens represents the Fourier spectrum of the object multiplied with a propagation term containing the object distance. The complex-valued field map is processed in the computer to numerically reconstruct the object.

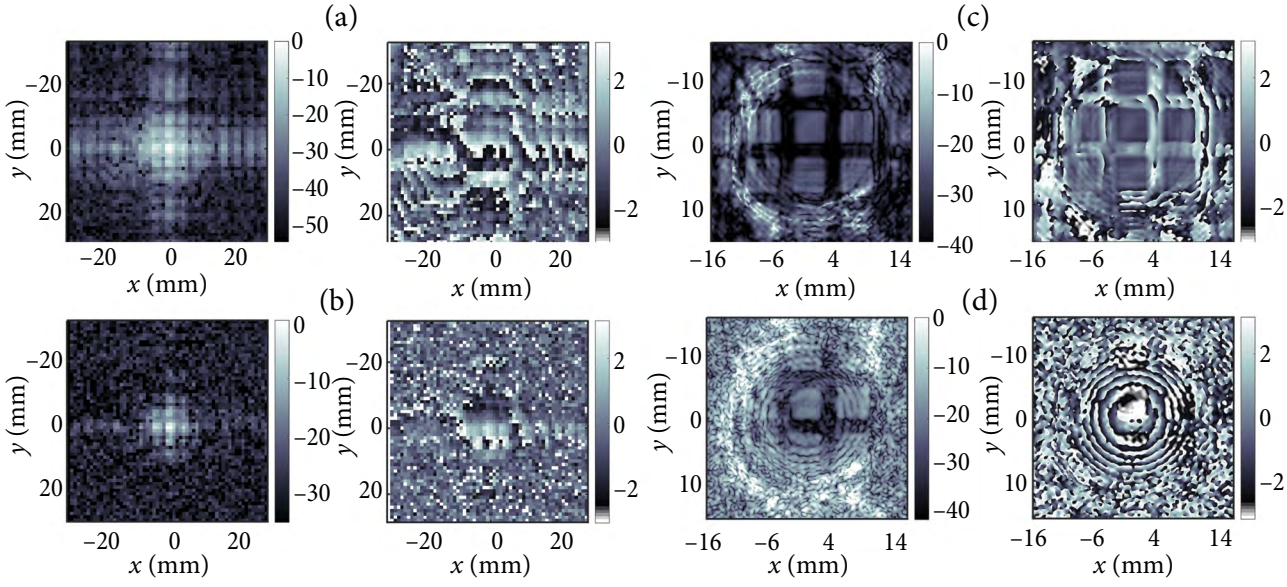


Fig. 5. Recorded Fourier-plane spectra ((a) and (b)) and reconstructed images ((c) and (d)). In all four quadrants, the left (right) panel displays the intensity (phase) distribution. Maps in the top row ((a) and (c)) are based on the measurements with the paraffin-wax superstrate lens. No superstrate lens for the bottom row ((b) and (d)).

superstrate lens. The increased sensitivity leads to a larger dynamic range of the detection for the same power values of the object-illuminating beam and the LO radiation.

It is worth pointing out that the reduced FOV, seen in Fig. 5, when the dynamic range is low, is a result of the illumination of the object with a collimated Gaussian beam. Its intensity decreases away from the optical axis. If one would detect the radiation directly behind the object instead of Fourier imaging, then it is obvious that detection with a low dynamic range leads to a small imaged area, as only a limited beam area around the optical axis has sufficient intensity for the detection above the noise floor. One obtains a truncated, small-FOV image of the object. Fourier imaging reproduces this behaviour, as it should, although it records the Fourier-plane spectrum and the image is reconstructed numerically.

Finally, we want to draw the reader's attention to Fig. 5(d). While the reconstructed intensity image in the left panel of Fig. 5(d) still retains recognizable information about the metal grid, the phase image in the right panel is nearly entirely buried by Gaussian noise. This finding is representative for many other observations, which we have made and which all indicate that the phase is more susceptible to noise in the Fourier-plane spectrum detection than the intensity. Great care has to be taken during the preparation of the measurement set-up, the beam alignment and the measurements themselves to avoid phase distortions because they can severely harm the image reconstruction.

## 6. Conclusions

In this article, we have revisited and explained our early developments of utilizing paraffin wax for the integration of superstrate lenses on THz semiconductor detectors. We have employed a time-domain THz spectroscopy system to measure the dielectric properties of paraffin wax in the THz band from 300 GHz to 1.5 THz. We have described the processing steps for the fabrication of superstrate lenses from paraffin wax on semiconductor detectors. In the form, as we have employed it, this is a manual process with a limited reproducibility. However, it has the overriding benefit that it allows one to place a superstrate lens onto the front-side of a detector, even if the detector surface is not smooth and even if bonding wires are in the way and render the use of unmodified solid immersion lenses difficult or impossible. The wax allows one to smoothen the surface, and to embed and protect the bonding wires before sculpturing the wax into the superstrate lens, as we have discussed in the present paper and in Ref. [17], or before attaching the lens made from another, solid material, as

we have done in Ref. [11]. The refractive index of paraffin wax at THz frequencies is comparable to those of materials such as PTFE, TPX and polypropylene, which makes the wax suitable as a dielectric material for the index-matched implementation of composite superstrate lenses. We have conducted coherent Fourier imaging experiments to validate the enhancement of the effective antenna area and the improved sensitivity predicted by theoretical considerations. For this purpose, a dual-lens-equipped TeraFET has been prepared. An all-wax superstrate lens has been used for the front-sided in-coupling of local-oscillator radiation, and a commercial Si substrate lens has been attached for the object-illuminating beam impinging from the backside. The coherent measurements have indeed shown that the application of the superstrate lens leads to an improved coupling efficiency of the local-oscillator radiation, translating into a better detection sensitivity, which plays a pivotal role for the imaging quality. With the lens, we have achieved a better dynamic range, an enhanced resolution and an expanded field-of-view.

## Acknowledgements

This work was funded by the German Research Foundation (DFG) under Grant RO 770/48-1. The authors would like to thank M. Zhang (General and Theoretical Electrical Engineering, University of Duisburg-Essen), M. Xiang, J. Holstein and L. Rößler (Physikalisches Institut, Goethe Universität Frankfurt am Main) for helpful discussions.

## References

[1] L. Cheng, W. Zhang, C. Li, Y. Ji, X. Liu, and G. Fang, HE-DETR-DC5 method to rapidly detect objects on passive THz images in human safety inspection, Electron. Lett. **59**(2), e12702 (2023), https://doi.org/10.1049/ell2.12702

[2] T. Amini, F. Jahangiri, Z. Ameri, and M.A. Hemmatian, A review of feasible applications of THz waves in medical diagnostics and treatments, J. Lasers Med. Sci. **12**(1), e92 (2021), https://doi.org/10.34172/JLMS.2021.92

[3] M. Karthikeya Sharma, A. Rao, K. Kumar, and T.R. Rao, Terahertz imaging for aerospace applications, in: *Proceedings of WiSPNET 2023 – International Conference on Wireless Communications, Signal Processing and Networking* (Institute of Electrical and Electronics Engineers Inc., 2023), https://doi.org/10.1109/WiSPNET57748.2023.10134245

[4] Y. Huang, Y. Shen, and J. Wang, From terahertz imaging to terahertz wireless communications, Engineering **22**, 106–124 (2023), https://doi.org/10.1016/j.eng.2022.06.023

[5] D.J. Yeong, G. Velasco-Hernandez, J. Barry, and J. Walsh, Sensor and sensor fusion technology in autonomous vehicles: A review, Sensors **21**(6), 2140 (2021), https://doi.org/10.3390/s21062140

[6] Y. Koyama, Y. Kitazawa, K. Yukimasa, T. Uchida, T. Yoshioka, K. Fujimoto, T. Sato, J. Iba, K. Sakurai, and T. Ichikawa, A high-power terahertz source over 10 mW at 0.45 THz using an active antenna array with integrated patch antennas and resonant-tunneling diodes, IEEE Trans. Terahertz Sci. Technol. **12**(5), 510–519 (2022), https://doi.org/10.1109/TTHZ.2022.3180492

[7] E. Javadi, D.B. But, K. Ikamas, J. Zdanevičius, W. Knap, and A. Lisauskas, Sensitivity of field-effect transistor-based terahertz detectors, Sensors **21**(9), 2909 (2021), https://doi.org/10.3390/s21092909

[8] F. Friederich, W. von Spiegel, M. Bauer, F. Meng, M.D. Thomson, S. Boppel, A. Lisauskas, B. Hils, V. Krozer, A. Keil, et al., THz active imaging systems with real-time capabilities, IEEE Trans. Terahertz Sci. Technol. **1**(1), 183–200 (2011), https://doi.org/10.1109/TTHZ.2011.2159559

[9] G. Valušis, A. Lisauskas, H. Yuan, W. Knap, and H.G. Roskos, Roadmap of terahertz imaging 2021, Sensors **21**(12), 4092 (2021), https://doi.org/10.3390/s21124092

[10] H. Yuan, D. Voß, A. Lisauskas, D. Mundy, and H.G. Roskos, 3D Fourier imaging based on 2D heterodyne detection at THz frequencies, APL Photonics **4**(10), 106108 (2019), https://doi.org/10.1063/1.5116553

[11] H. Yuan, A. Lisauska, M. Zhang, Q. ul-Islam, D. Erni, and H.G. Roskos, Fourier imaging based on sub-harmonic detection at 600 GHz, in: *Proceedings of the 2022 Fifth International Workshop on Mobile Terahertz Systems (IWMTS)*

(2022) pp. 1–4, https://doi.org/10.1109/IWMTS54901.2022.9832459

[12] R.I. Stantchev, X. Yu, T. Blu, and E. Pickwell-MacPherson, Real-time terahertz imaging with a single-pixel detector, Nat. Commun. **11**(1), 2535 (2020), https://doi.org/10.1038/s41467-020-16370-x

[13] J. Grzyb and U. Pfeiffer, THz direct detector and heterodyne receiver arrays in silicon nanoscale technologies, J. Infrared Millim. Terahertz Waves **36**(10), 998–1032 (2015), https://doi.org/10.1007/s10762-015-0172-6

[14] D. Glaab, S. Boppel, A. Lisauskas, U. Pfeiffer, E. Öjefors, and H.G. Roskos, Terahertz heterodyne detection with silicon field-effect transistors, Appl. Phys. Lett. **96**(4), 042106 (2010), https://doi.org/10.1063/1.3292016

[15] S. Boppel, A. Lisauskas, A. Max, V. Krozer, and H.G. Roskos, CMOS detector arrays in a virtual 10-kilopixel camera for coherent terahertz real-time imaging, Opt. Lett. **37**(4), 536–538 (2012), https://doi.org/10.1364/OL.37.000536

[16] H. Yuan, A. Lisauskas, M.D. Thomson, and H.G. Roskos, 600-GHz Fourier imaging based on heterodyne detection at the 2nd sub-harmonic, Opt. Express **31**, 40856-40870 (2023), https://doi.org/10.1364/OE.487888

[17] H. Yuan, A. Lisauskas, M. Zhang, A. Rennings, D. Erni, and H.G. Roskos, Dynamic-range enhancement of heterodyne THz imaging by the use of a soft paraffin-wax substrate lens on the detector, in: *Proceedings of the 2019 Photonics & Electromagnetics Research Symposium – Fall (PIERS – Fall)* (IEEE, 2019) pp. 2607–2611, https://doi.org/10.1109/PIERS-Fall48861.2019.9021735

[18] M. Freund and G. Mózes, *Paraffin Products: Properties, Technologies, Applications* (Elsevier Scientific Pub. Co., 1982).

[19] Q. ul-Islam, F. Meng, M.D. Thomson, and H.G. Roskos, Terahertz photoconductive waveguide emitter with excitation by a tilted optical pulse front, Opt. Express **28**(22), 33673–33681 (2020), https://doi.org/10.1364/OE.403161

[20] W. Cai and V. Shalaev, *Optical Metamaterials: Fundamentals and Applications* (Springer, New York, 2010), https://doi.org/10.1007/978-1-4419-1151-3

[21] P.U. Jepsen, D.G. Cooke, and M. Koch, Terahertz spectroscopy and imaging – Modern techniques and applications, Laser Photon Rev. **5**(1), 124–166 (2011), https://doi.org/10.1002/lpor.201000011

[22] M. Bauer, A. Rämer, S.A. Chevtchenko, K.Y. Osipov, D. Cibiraite, S. Pralgauskaite, K. Ikamas, A. Lisauskas, W. Heinrich, V. Krozer, and H.G. Roskos, A high-sensitivity AlGaN/GaN HEMT terahertz detector with integrated broadband bow-tie antenna, IEEE Trans. Terahertz Sci. Technol. **9**(4), 430–444 (2019), https://doi.org/10.1109/TTHZ.2019.2917782

[23] S. Boppel, A. Lisauskas, D. Seliuta, L. Minkevičius, I. Kašalynas, G. Valušis, V. Krozer, and H.G. Roskos, CMOS integrated antenna-coupled field-effect transistors for the detection of radiation from 0.2 to 4.3 THz, IEEE Trans. Microw. Theory Tech. **60**(12), 3834–3843 (2012), https://doi.org/10.1109/TMTT.2012.2221732

[24] M. Asada, Theoretical analysis of subharmonic injection locking in resonant-tunneling-diode terahertz oscillators, Jpn. J. Appl. Phys. **59**(1), 018001 (2020), https://doi.org/10.7567/1347-4065/ab600b

[25] *Infrared and Millimeter Waves, Volume 10 – Millimeter Components and Techniques Part II,* ed. K. J. Button (Academic Press, INC, 1983), https://books.google.de/books?hl=en&lr=&id=delnT8ewgT4C&oi=fnd&pg=PA1&dq=integrated+circuit+antennas&ots=4rkEya4-pS&sig=7LaDqfshNEFovf7Nd32nfdyra5U#v=onepage&q=integrated%20circuit%20antennas&f=false

[26] C. Rønne, L. Thrane, P.O. Åstrand, A. Wallqvist, K.V. Mikkelsen, and S.R. Keiding, Investigation of the temperature dependence of dielectric relaxation in liquid water by THz reflection spectroscopy and molecular dynamics simulation, J. Chem. Phys. **107**(14), 5319–5331 (1997), https://doi.org/10.1063/1.474242

[27] A. Lisauskas, S. Boppel, M. Mundt, V. Krozer, and H.G. Roskos, Subharmonic mixing with field-effect transistors: Theory and experiment at 639 GHz high above $f_T$, IEEE Sens. J. **13**(1),

124–132 (2012), https://doi.org/10.1109/jsen.2012.2223668

[28] A. Lisauskas, U. Pfeiffer, E. Öjefors, P. Haring Bolivar, D. Glaab, and H.G. Roskos, Rational design of high-responsivity detectors of terahertz radiation based on distributed self-mixing in silicon field-effect transistors, J. Appl. Phys. **105** (11), 114511 (2009), https://doi.org/10.1063/1.3140611

[29] K. Ikamas, D. Čibiraitė, A. Lisauskas, M. Bauer, V. Krozer, and H.G. Roskos, Broadband terahertz power detectors based on 90-nm silicon CMOS transistors with flat responsivity up to 2.2 THz, IEEE Electron Device Lett. **39**(9), 1413–1416 (2018), https://doi.org/10.1109/LED.2018.2859300

## PAVIRŠINIO LĘŠIO INTEGRAVIMAS ANT PUSLAIDININKINIŲ TERAHERCINIŲ DETEKTORIŲ LUSTŲ PANAUDOJANT PARAFINO VAŠKĄ

H. Yuan, Q. ul-Islam, H.G. Roskos

*Frankfurto prie Maino Johano Volfgango Gėtės universiteto Fizikos institutas, Frankfurtas prie Maino, Vokietija*

**Special dedication to prof. Gintaras Valušis**

Our article is dedicated to Prof. Dr. Gintaras Valušis on the occasion of his 60th birthday. In gratitude for many years – by now decades – of cooperation, mutual support, respect and friendship. Our interaction has led to many papers which we have published together. I myself, being four years his senior, have seen him growing from an adventurous post-doc, who established the 'THz Atelier' as an innovative and internationally well-connected THz device research lab in the Semiconductor Physics Institute at Goštauto 11, Vilnius, to becoming the director of the Center for Physical Sciences and Technology, which was founded in 2010. Prof. Valušis was instrumental in developing the new premises of the Centre at Saulėtekio 3, Vilnius. This important task with its enormous responsibilities took its toll, turning Prof. Valušis' hair white in a short period of time. Since then, he has not taken the probable course of life to turn into a full-time administrator, but he has retained his passion for actively and vigorously pursuing research, which has led to highly recognized publications in the field of THz science especially in recent years.

With our contribution to this special edition of the *Lithuanian Journal of Physics*, we honor Gintaras Valušis and wish him fulfilling and successful years of leadership and active research to come. And personally, I wish that our friendship continues and thrives.

Prof. Dr. Hartmut Roskos
Johann Wolfgang Goethe-Universität
Frankfurt am Main, Germany